International Journal of Minerals, Metallurgy and Materials
Volume 19, Number 7, July 2012, Page 657
DOI: 10.1007/s12613-012-0609-z

Microstructure and corrosion resistance of Fe/Mo composite amorphous coatings prepared by air plasma spraying

Chao-ping Jiang, Ya-zhe Xing, Feng-ying Zhang, and Jian-min Hao

Engineering Research Center of Transportation Materials (Ministry of Education), School of Materials Science and Engineering, Chang'an University, Xi'an 710064, China

(Received: 14 December 2011; revised: 3 March 2012; accepted: 6 March 2012)

Abstract: Fe/Mo composite coatings were prepared by air plasma spraying (APS) using Fe-based and Mo-based amorphous and nanocrystalline mixed powders. Microstructural studies show that the composite coatings present a layered structure with low porosity due to adding the self-bonded Mo-based alloy. Corrosion behaviors of the composite coatings, the Fe-based coatings and the Mo-based coatings were investigated by electrochemical measurements and salt spray tests. Electrochemical results show that the composite coatings exhibit a lower polarization current density and higher corrosion potentials than the Fe-based coating when tested in 3.5wt% NaCl solutions, indicating superior corrosion resistance compared with the Fe-based coating. Also with the increase in addition of the Mo-based alloy, a raised corrosion resistance, inferred by an increase in corrosion potential and a decrease in polarization current density, can be found. The results of salt spray tests again show that the corrosion resistance is enhanced by adding the Mo-based alloy, which helps to reduce the porosity of the composite coatings and enhance the stability of the passive films.

Keywords: composite coatings; plasma spraying; amorphous; corrosion resistance; microstructure

[*This work was financially supported by the Special Fund for Basic Scientific Research of Central Colleges, Chang'an University (No. CHD2011JC126), the Special Fund for Basic Research Support Plan of Chang'an University, and the Open Fund of the Engineering Research Center of Transportation Materials, Ministry of Education of China.*]

1. Introduction

Air plasma spraying (APS) coatings have been widely used for industrial applications where good wear or corrosion resistance are needed exigently, because this technology has the characteristic of the high cooling rate of 10^5-10^7 $K \cdot s^{-1}$, which can be used to fabricate amorphous coatings [1-4]. Fe-based amorphous metallic glasses are considered to be extremely viable candidates as surface protective coatings owing to their high crystallization temperature, superior corrosion and wear resistance, good magnetic properties, and relatively low material cost [5-7]. However, amorphous phase is a non-equilibrium phase, so alloys with high glass-forming ability (GFA) would be favorable for forming and retaining fully amorphous phase coatings via APS process. Recently, a series of Fe-based bulk metallic glasses with high GFA have been found in Fe-(Cr,Mo)-(C,B) alloy systems, leading to obtain amorphous metallic coatings more easily for satisfying engineering needs [8-9]. The previous study suggested that the element constituents and the chemical composition of the alloys affect the corrosion resistance of the glassy alloys [10]. Much research has been focused on various base elements such as Fe, Zr, Cu, and Ni as well as their optimum chemical compositions [11-13]. The super corrosion resistance of Ni-based coatings demonstrated that element Ni could enrich a stable passive film [14].

In this paper, in order to improve the corrosion resistance of $Fe_{74}Cr_7Mo_3Ni_3Si_2BP_6C_4$ amorphous coatings, $Mo_{63}Ni_{25}Cr_6Si_2Fe_2BP$ amorphous and nanocrystalline powders with

Corresponding author: Chao-ping Jiang E-mail: jcp100415@126.com

high Mo and Ni contents were added into Fe-based amorphous powders to deposit Fe/Mo composite coatings by APS. The microstructure and corrosion behaviors of the composite coatings were investigated in detail.

2. Experimental

$Fe_{74}Cr_7Mo_3Ni_3Si_2BP_6C_4$ and $Mo_{63}Ni_{25}Cr_6Si_2Fe_2BP$ alloy powders were employed as thermal spray materials obtained by gas atomization in an argon atmosphere. The mixed powders, with different Mo-based powders contents of 9wt%, 17wt%, and 23wt%, were named A-1, A-2, and A-3, respectively. Before spraying, the mixed powders were ball-milled for about 2 h. A rectangular 45# steel plate with a size of 30 mm×15 mm×3 mm was used as the substrate. Prior to spraying, the substrate was degreased in acetone and grit blasted using virgin brown alumina particles with an average diameter of 1-3 mm.

A GP-80 APS system was used to spray the coatings. Argon was used as the primary gas, and nitrogen was used as the auxiliary gas. The pressures of both argon and nitrogen were operated at 0.7 and 0.68 MPa, respectively, during spraying. The flow of the primary gas was fixed to 60 L/min, and that of the auxiliary gas was fixed to 6 L/min. Argon was used as the powder feed gas and the powder feed rate was 10 g/min. Plasma jet was operated to deposit the coatings at a power level of 20 kW (400 A/50 V). The spraying distance was 100 mm. During the plasma spraying process, the powders were fed to the spray gun, heated to the molten or semi-molten states, and then accelerated toward the substrate.

The microstructure of the coatings after salt spray test was characterized by scanning electron microscopy (SEM, S-4800). X-ray diffraction (XRD, X'Pert Pro) analyses of the powders and coatings were performed on an X-ray diffractometer with Cu K_α radiation. The corrosion behavior of the coatings was evaluated by electrochemical measurements and salt spray test. Prior to the corrosion test, all samples were wet-ground to 1200 grit using SiC paper. The samples for the corrosion test were closely sealed with epoxy resin, leaving only an end-surface (with a surface area of 1 cm^2) exposed for testing. The potentiodynamic polarization experiments were performed at room temperature in 3.5wt% NaCl solutions, which simulated seawater. The salt spray test was carried on for 168 h long in 5wt% NaCl solutions. After salt spray test, the coating surfaces were analyzed by optical microscopy (OM, LWM300LJT) and SEM.

3. Results and discussion

3.1. Structures and morphologies of the coatings

Fig. 1 presents typical cross-section morphologies of the composite coatings, Fe-based coatings and Mo-based coatings prepared by APS. Generally, all samples show a typical lamellar structure of plasma sprayed coatings where the

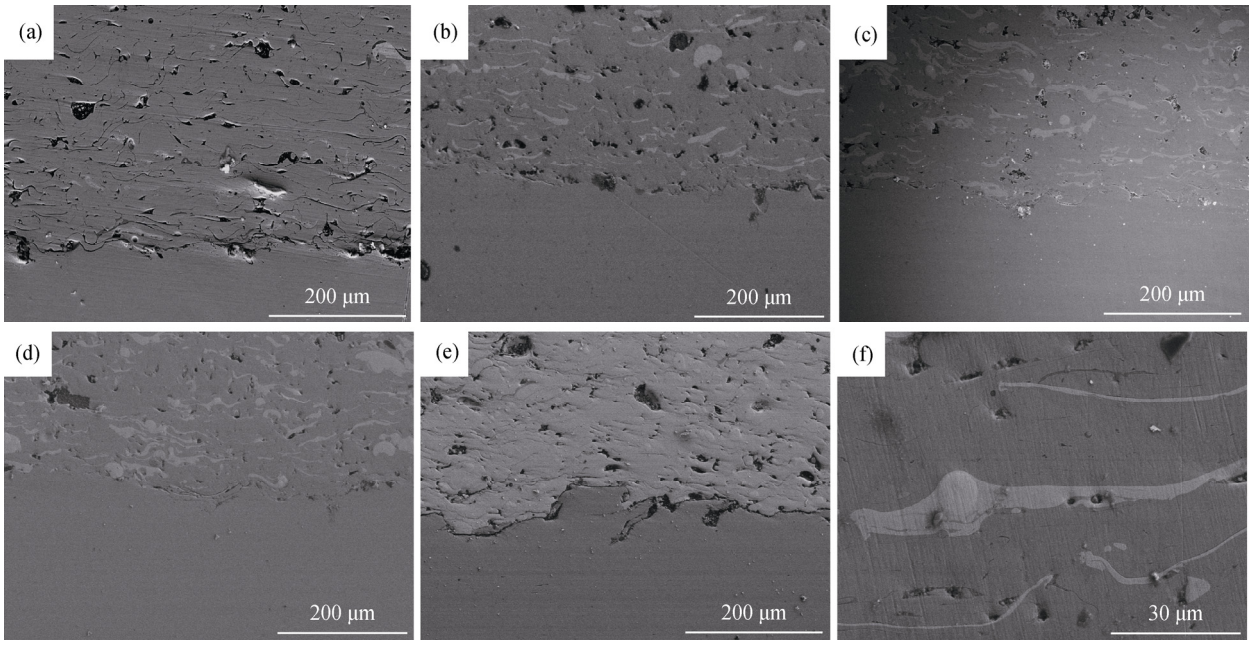

Fig. 1. Cross-sectional backscattered SEM micrographs of coatings: (a) Fe-based; (b) A-1; (c) A-2; (d) A-3; (e) Mo-based; (f) blowup part of A-3.

sprayed powders deformed and solidified when they impinged on the substrate surface to form splats. The splats piled up during spraying to gain the coating thickness. Some pores and microcracks exist as very dark regions can be seen from the images. Compared with the Fe-based coating (Fig. 1(a)), the Mo-based coating (Fig. 1(e)) is denser, identified as a lower porosity due to its self-bonding characteristic.

From Figs. 1(b)-1(d), some light grey phases indicate that Mo alloy splats appeared in the composite coatings. At the same time, more and more Mo alloy splats appeared in the coatings with increasing Mo-based powders proportion. The Mo-based splats take the place of Fe-based splats in the composite coating, which decrease the exposure area of Fe-based splats on the coating surface correspondingly. There is no separation between these splats with different materials due to the self-bonding property of the Mo alloy, meaning that intersplat chemical bonding forms within the coatings [15]. Therefore, the Mo alloy splats can bond strongly with the Fe alloy splats, forming a low porosity coating with good integrity, as shown in Fig. 1(f).

3.2. XRD analysis

Fig. 2 presents the XRD patterns of the two atomized powders, which indicate their partially amorphous phase structure. The only diffraction peak in the Fe-based powders corresponds to Fe phase. The Mo-based coating has crystalline phases of Mo, MoB, $Fe_{0.54}Mo_{0.73}$, and Fe_3B.

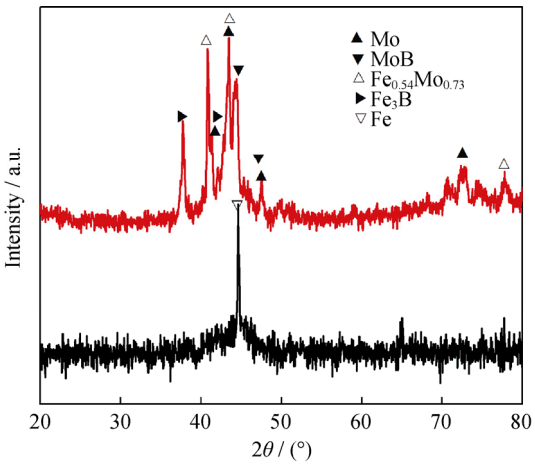

Fig. 2. XRD patterns of Fe-based and Mo-based atomized powders.

Fig. 3 shows the XRD patterns of the Fe-based, composite, and Mo-based coatings. It is notable that a single broad halo peak appears in the Fe-based coating and the composite coatings, indicating their high amorphous phase content, which is attributed to the quick heating and cooling characteristic of APS process. Although the Mo-based coating has some crystalline peaks, the number of diffraction peaks is much less than that of the powders. The main crystalline phases in the Mo-based coating are Mo and FeCrMo. According to the Scherrer formula, the measured grain size of the Mo-based coating is about 100 nm, indicating that the Mo-based coating includes some nanocrystalline phases besides amorphous phase.

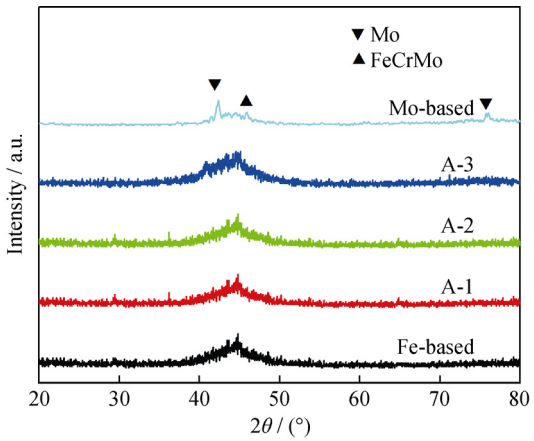

Fig. 3. XRD patterns of the Fe-based, composite, and Mo-based coatings.

3.3. Electrochemical corrosion behaviors of the coatings

Fig. 4 shows the potentiodynamic polarization plots of the Fe-based, composite, and Mo-based coatings deposited by APS process at room temperature. The corrosion potentials and polarization current density of different coatings are listed in Table 1. It can be seen that the Mo-based amorphous nanocrystalline coating exhibits spontaneous passivation with a higher corrosion potential and a relatively lower polarization current density of about 61.2 μA/cm^2. The Mo-based coating has a wide passive region, which

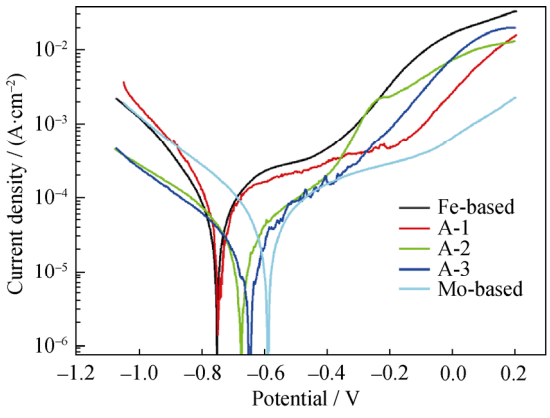

Fig. 4. Potentiodynamic polarization curves of the coatings in 3.5wt% NaCl solutions.

Table 1. Corrosion potentials and polarization current densities of the coatings

Sample	Corrosion potential / V	Current density / ($\mu A \cdot cm^{-2}$)
Fe-based	–0.75	150.0
A-1	–0.74	96.3
A-2	–0.68	45.9
A-3	–0.65	21.5
Mo-based	–0.57	61.2

suggests that this coating has a prominent ability to resist localized corrosion. Passivation also appears in the Fe-based coating, only its corrosion potential shows more negative, and the polarization current density is higher comparatively. The polarization current density of the Fe-based coating is 150.0 $\mu A/cm^2$, which is higher than the double value of the Mo-based coating.

The polarization curves also clearly reveal the fact that with the Mo alloy powders added the passive regions of the composite coating become wider and the polarization currents turn to lower. The A-1 coating has a larger passive region width (from –0.65 to –0.2 V), which is attributed to the improvement in stability of the passive film by Mo alloy addition. The polarization current density of A-1 is 96.3 $\mu A/cm^2$, which is much lower than the Fe-based coating. The A-3 coating exhibits passivation with low polarization current density (21.5 $\mu A/cm^2$), which is attributed to that self-bonded Mo enhances the compactness and stability of the coating and enables the formation of a uniform passivation film easily.

3.4. Salt spray test of the coatings

From the potentiodynamic behavior, it is clear that the Mo-based and composite coatings show a higher corrosion resistance than the Fe-based coating in NaCl solution, so this encourages us to study the corrosion behaviors of these coatings by salt spray test. Figs. 5 and 6 show the OM and SEM photographs of the coating surfaces after salt spray test. In the Fe-based coating, there is much rust distributing in the coating surface, especially in the regions where pores and cracks exist (see Figs. 5(a) and 6(a)). The chemically inhomogeneous surface and the difference in thickness of the passive layer could be favorable sites for the adsorption of chloride ions, leading to the breaking of passive layers that would result in an easy dissolution of the metal [12]. Therefore, pores and cracks can do harm to passive film forming and repairing.

The corrosion behaviors of the composite coatings are given in Figs. 5(b)-(d) and 6(b)-6(d). With the increase of Mo-based alloy content in the composite coatings, there is less pitting on the surface of the coating with the dense coating formed. The Mo alloy can enhance the stability of the passive film with very low polarization current density. It is obvious that the corrosion starts at the pores where primary cells are formed easily.

There are few rusts in the Mo-based coating, as shown in Figs. 5(e) and 6(e). The Mo-based coating shows a good corrosion resistance in NaCl solution for it contains elements such as Ni, Cr, and P. It is understood that, irrespective of the amorphous structure formed, the discrepancy in

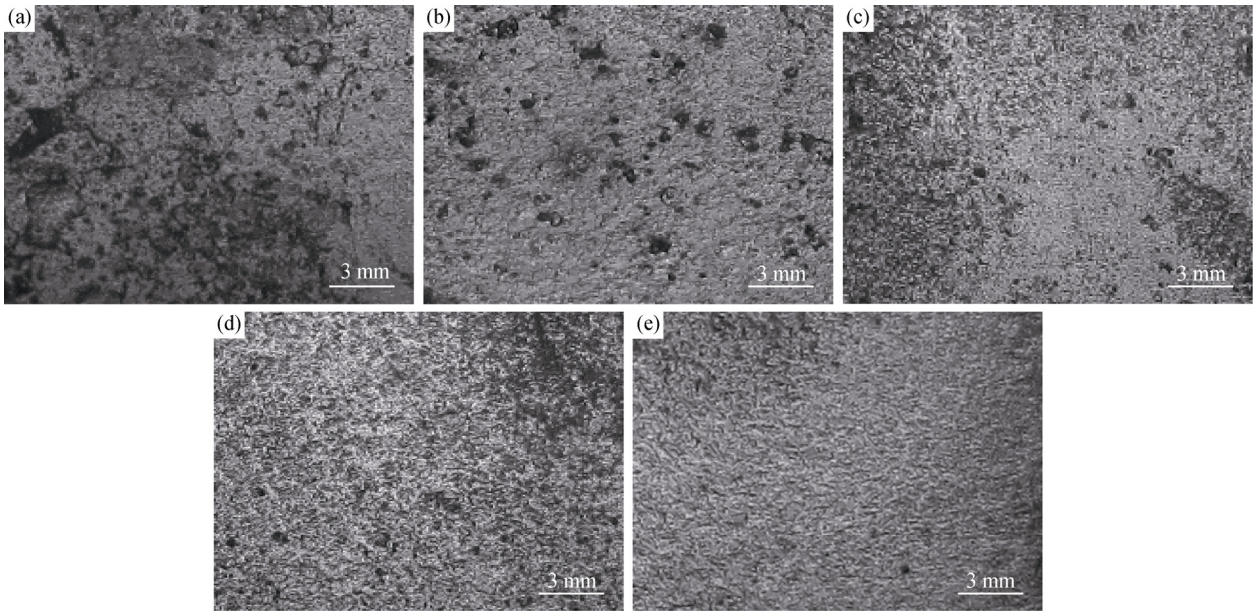

Fig. 5. OM photographs of the coating surfaces after salt spray test: (a) Fe-based; (b) A-1; (c) A-2; (d) A-3; (e) Mo-based.

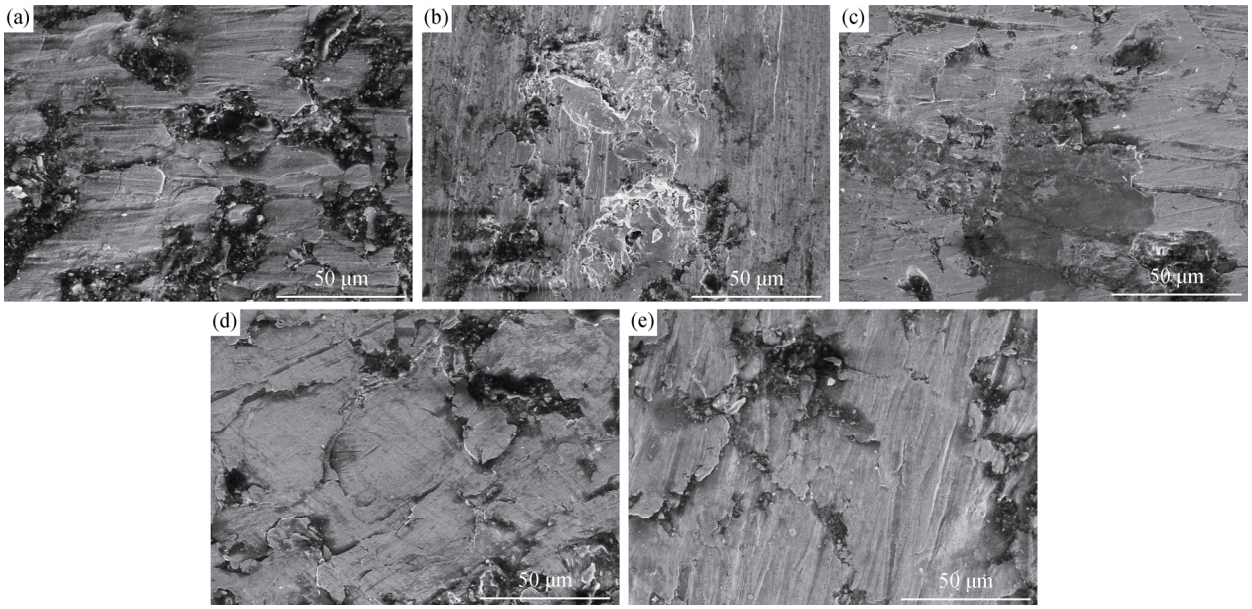

Fig. 6. SEM photographs of the coating surfaces after salt spray test: (a) Fe-based; (b) A-1; (c) A-2; (d) A-3; (e) Mo-based.

the corrosion behavior in NaCl solution can be attributed to the content of high corrosive resistance alloy elements such as Ni, Cr, Mo, and Ta [16]. The concentration of Cr at the surface of the passive film is increased by the addition of Mo in alloy since it prevents the dissolution of chromium during passivation [17].

4. Conclusions

The presence of Mo splats in the composite coating can help reduce the area of the Fe-based alloy comparatively. For the Mo self-bonding properties, a denser coating was obtained with mixed powders by APS process compared with the coating without Mo addition. The corrosion resistance of the composite coatings is dependent on the proportion of added Mo-based powders. When the amount of the Mo-based alloy is low in the A-1 coating, the passive films break down and dissolve easily because pores deteriorate the integrity of the coating surface and the role of the Mo alloy cannot take effect. The A-3 coating with adding about 23% of the Mo-based alloy shows good corrosion resistance due to many Mo-based splats that appear on the surface of the coating, which can enhance the stability of the passive film and delay its dissolution.

References

[1] Z. Zhou, L. Wang, F.C. Wang, H.F. Zhang, Y.B. Liu, and S.H. Xu, Formation and corrosion behavior of Fe-based amorphous metallic coatings by HVOF thermal spraying, *Surf. Coat. Technol.*, 204(2009), p.563.

[2] A. Singh, S.R. Bakshi, A. Agarwal, and S.P. Harimkar, Microstructure and tribological behavior of spark plasma sintered iron-based amorphous coatings, *Mater. Sci. Eng. A*, 527(2010), p.5000.

[3] M. Li and P.D. Christofides, Multi-scale modeling and analysis of an industrial HVOF thermal spray process, *Chem. Eng. Sci.*, 60(2005), p.3649.

[4] Y.Y. Wang, C.J. Li, and A. Ohmori, Influence of substrate roughness on the bonding mechanisms of high velocity oxy-fuel sprayed coatings, *Thin Solid Films*, 485(2005), p.141.

[5] A. Inoue, B.L. Shen, and C.T. Chang, Super-high strength of over 4000 MPa for Fe-based bulk glassy alloys in $[(Fe_{1-x}Co_x)_{0.75}B_{0.2}Si_{0.05}]_{96}Nb_4$ system, *Acta Mater.*, 52(2004), p.4093.

[6] Z. Zhou, L. Wang, D.Y. He, F.C. Wang, and Y.B Liu, Microstructure and electrochemical behavior of Fe-based amorphous metallic coatings fabricated by atmospheric plasma spraying, *J. Therm. Spray Technol.*, 20(2011), p.344.

[7] W.H. Lu, Y.P. Wu, J.J. Zhang, S. Hong, J.F. Zhang, and G.Y. Li, Microstructure and corrosion resistance of plasma sprayed Fe-based alloy coating as an alternative to hard chromium, *J. Therm. Spray Technol.*, 20(2011), p.1063.

[8] V. Ponnambalam, S.J. Poon, and G.J. Shiflet, Fe-Mn-Cr-Mo-(Y,Ln)-C-B (Ln=Lanthanides) bulk metallic glasses as formable amorphous steel alloys, *J. Mater. Res.*, 19(2004), p.3046.

[9] C.S. Kiminami, C.A.C. Souza, L.F. Bonavina, L.R.P. de Andrade Lima, S. Suriñach, M.D. Baró, C. Bolfarini, and W.J. Botta, Partial crystallization and corrosion resistance of amorphous Fe-Cr-M-B (M=Mo, Nb) alloys, *J. Non Cryst.*

Solids, 356(2010), p.2651.

[10] P.L. Zhang, H. Yan, C.W. Yao, Z.G. Li, Z.S. Yu, and P.Q. Xu, Synthesis of Fe-Ni-B-Si-Nb amorphous and crystalline composite coatings by laser cladding and remelting, *Surf. Coat. Technol.*, 206(2011), p.1229.

[11] Y.H. Yoo, S.H. Lee, J.G. Kim, J.S. Kim, and C. Lee, Effect of heat treatment on the corrosion resistance of Ni-based and Cu-based amorphous alloy coatings, *J. Alloys Compd.*, 461(2008), p.304.

[12] R.Q. Guo, C. Zhang, Q. Chen , Y. Yang, N. Li, and L. Liu, Study of structure and corrosion resistance of Fe-based amorphous coatings prepared by HVAF and HVOF, *Corros. Sci.*, 53(2011), p.2351.

[13] L. Liu, C.L. Qiu, Q. Chen, and S.M. Zhang, Corrosion behavior of Zr-based bulk metallic glass in different artificial body fluids, *J. Alloys Compd.*, 425(2006), p.268.

[14] W.X. Zhang, Z.H. Jiang, G.Y. Li, Q. Jiang, and J.S. Lian, Electroless Ni-Sn-P coating on AZ91D magnesium alloy and its corrosion resistance, *Surf. Coat. Technol.*, 202(2008), p.2570.

[15] P. Niranatlumpong and H. Koiprasert, The effect of Mo content in plasma-sprayed Mo-NiCrBSi coating on the tribological behavior, *Surf. Coat .Technol.*, 205(2010), p.483.

[16] S. Pang, T. Zhang, K. Asami, and A. Inoue, Bulk glassy Ni(Co-)Nb-Ti-Zr alloys with high corrosion resistance and high strength, *Mater. Sci. Eng. A*, 375-377(2004), p.368.

[17] J. Kawakita, S. Kuroda, T. Fukushima, and T. Kodama, Improvement of corrosion resistance of high-velocity oxy-fuel-sprayed stainless steel coatings by addition of molybdenum, *J. Therm. Spray Technol.*, 14(2005), p.224.